Influence of Boundaries of Nanoporous Crystals on Molecular Exchange under the Conditions of Single-File Diffusion

Andreas Schüring,*,†,‡ Sergey Vasenkov,‡ and Siegfried Fritzsche†

Universität Leipzig, Institut für Theoretische Physik, Augustusplatz 10-11, D-04109 Leipzig, Germany, and Universität Leipzig, Institut für Experimentelle Physik I, Linnéstr. 5, D-04103 Leipzig, Germany

Received: May 4, 2005; In Final Form: July 13, 2005

We study the tracer exchange of molecules between the phase adsorbed in one-dimensional channels and the surrounding gas phase by molecular dynamics simulations. Under the conditions of single-file diffusion, a novel boundary effect is observed. The shape of the tracer-exchange concentration profiles *deviates* from those obtained under the conditions of normal diffusion. Compared to the profiles for normal diffusion, which correspond to the same degree of exchange, the equilibrium concentration is reached faster at the boundaries and slower in the middle part of the channel in the case of single-file diffusion. This boundary effect is observed for the system neopentane in $AlPO_4$-5 (which was chosen as a reference system), as well as for modified systems. The effect can be understood considering two diffusion mechanisms which occur in parallel. First, the diffusion of the whole chain of particles, that is, the center-of-mass diffusion, obeying the laws of normal diffusion. Second, the individual movement of the particles relative to the center of mass of the chain. The second mechanism admits additional displacements which, on average, lead to an accelerated exchange of the marginal particles.

1. Introduction

Single-file diffusion (SFD), that is, the transport of molecules or particles in one-dimensional systems of narrow channels where mutual passages are excluded, has received over the last years renewed attention of the scientific community due to the importance of this process for many recently discovered systems such as zeolites,[1] nanotubes,[2] and ion channels in cell membranes.[3] Recent attempts to observe SFD experimentally have resulted in a number of highly interesting publications, which, at least in some cases, provide clear evidence of the occurrence of SFD.[4−8] The most recent examples include observations of SFD of colloidal particles confined in topographical channels and in channels created by optical tweezers.[7,8]

A high degree of correlation between the movements of individual particles in infinite single-file systems renders Fick's laws to be inapplicable. In contrast to the prediction of Fick's laws, the mean square displacement (MSD) of diffusing species in such systems for large diffusion times grows as the square root of time[9−11]

$$\langle z^2(t)\rangle = 2F\sqrt{t} \tag{1}$$

where F is the mobility factor and t is the diffusion time. It was recently shown by using analytical models as well as molecular dynamics (MD) and dynamic Monte Carlo (MC) simulations that, in an interval of sufficiently small times, eq 1 is also valid for diffusion in finite single-file systems.[12−17] However, at times larger than the certain crossover time, t_c, discussed in refs 13 and 14, the MSD becomes proportional to t as required by the laws of "normal" diffusion[13,14,16,18]

$$\langle z^2(t)\rangle = 2D_s t \tag{2}$$

where the diffusivity D_s can be associated with the motion of the center of mass of particles in a finite single-file system. Such motion requires correlated displacements of all particles in any particular channel. In the limit of fast exchange between the channel margins and the surroundings and far away from the margins, the diffusivity D_s can be presented as[13,14]

$$D_s = \frac{(1-\theta)D_0}{L\theta} \tag{3}$$

where D_0 denotes the diffusion coefficient of molecules in the case of normal diffusion at infinite dilution, θ is the fraction of adsorption sites which are occupied by molecules, and L is the number of sites in the channel.

Despite the importance of the knowledge of the time dependence of the MSD far from the channel margins, this knowledge alone is not sufficient to describe all relevant properties of finite single-file systems. In particular, a fundamental understanding of the process of tracer exchange (viz., molecular exchange under the conditions of sorption equilibrium) between zeolite crystals possessing single-file channels and their surroundings requires exact knowledge of the transport properties and of the intracrystalline concentration profiles of tracer molecules near boundaries of zeolite crystals. It has recently been shown by using dynamic MC simulations[19] that under the conditions of tracer exchange the concentration profiles of labeled molecules (i.e., the molecules located in single-file channels at the time of the start of the tracer-exchange process) far from the boundaries of a finite single-file system can be well described by the corresponding solutions of Fick's laws with the diffusivity close to D_s. At the same time, the profiles obtained from the simulations in the regions near the boundaries have been found to deviate significantly from those

* To whom correspondence should be addressed. E-mail: aschu@pcserv.exphysik.uni-leipzig.de. Phone: ++49 341 2352589. Fax: ++49 341 2352307.

† Institut für Theoretische Physik.

‡ Institut für Experimentelle Physik I.

10.1021/jp052314k CCC: $30.25
Published on Web 08/16/2005

predicted by Fick's laws.[19] In these regions, the equilibrium occupancy of the single-file channels by the labeled and by the unlabeled molecules is achieved long before such equilibrium can be established in the case of normal diffusion with the diffusivity D_s. This results in "flat" concentration profiles of the labeled (unlabeled) molecules near the boundaries of single-file systems. Qualitatively similar boundary effects have also been observed for the case of tracer counterpermeation in single-file systems studied by the dynamic MC method.[18]

In this paper, we report the results of the investigation of molecular exchange between zeolite crystals and their surroundings under conditions of SFD for several model zeolite systems by using the MD method. Particular attention has been given to the influence of boundaries of zeolite crystals on the tracer-exchange process. This study is motivated by the recent trend in material science and catalysis aiming at the development of hybrid materials, which contain small, nanosized zeolite crystals and transport mesopores allowing fast access of large guest molecules to zeolite micropores.[20,21] Extremely large surface-to-volume ratios of zeolite nanocrystals in such hybrid materials obviously lead to an increased importance of molecular transport through crystal margins. Therefore, the boundary effects studied in the present work are expected to play an especially large role for these novel materials.

2. Simulations

This paper is devoted to the study of tracer exchange in macroscopic single-file sytems such as zeolite crystals. This process happens on a time scale larger than several microseconds. To be able to perform MD simulations on this time scale, a simple model of the system is needed. Therefore, we neglect the dynamic processes happening on a short time scale, that is, vibrations of the guest molecules and of the lattice atoms of the adsorbent as well as the rotation of the molecules. For these reasons, the guest molecules are approximated as spherical particles. We restrict the model to the properties which are relevant for the dynamic events on a long time scale; that is, the potential energy landscape for the spherical adsorbate molecules in the adsorbent is characterized by (1) an adsorption energy for the molecules in the channel, (2) potential barriers in the channel between adsorption sites, (3) an attractive outer surface of the adsorbent, and (4) a negligibly small interaction force between the adsorbent and the adsorbate located in the gas phase region.

Furthermore, it is our aim to find the relations between these (especially the first two) properties of the system and the diffusional properties of the adsorbed particles. For this reason, we have studied tracer exchange using variations of the reference potential (neopentane in $AlPO_4$-5) representing different physical situations.

The reference system used consists of neopentane molecules adsorbed in the channels of the aluminophosphate material $AlPO_4$-5. In the model-building procedure, the neopentane molecule, $C(CH_3)_4$, is reduced to a spherical Lennard-Jones particle moving in the potential of the zeolite atoms. In a second step, the potential energy landscape of the spherical particle in the channel is mapped to an analytical function of the potential energy. For additional simulations representing different physical situations, the parameters of the analytical potential energy function are varied. A detailed description of these single steps of the model-building procedure is given in the following sections.

2.1. Model of $AlPO_4$-5. The aluminophosphate $AlPO_4$-5 was chosen as a representation of a one-dimensional channel system. The channels of $AlPO_4$-5 are directed along the crystallographic direction z and have a free diameter of approximately 0.73 nm.[1] The neopentane molecules, which have a diameter of $\approx$0.5 nm, have a vanishing probability to pass each other within the channel.

The actual crystal structure of $AlPO_4$-5 is far from being simple. In particular, intergrowth effects may frequently occur in AFI-type crystals, as has been recently shown by using interference microscopy.[22,23] Furthermore, modulations of the positions of the oxygen atoms in the lattice have been reported.[24,25] Deviations from the ideal structure can also be expected for other real single-file systems. However, for the simulations presented here, an idealized structure was used which offers the possibility to study the properties of interest in the absence of additional disturbing effects.

The lattice atom positions were chosen in hexagonal symmetry with unit-cell constants $a = 1.3726$ nm and $c = 0.8484$ nm[1] and are given in the Supporting Information for this paper. The distance between opposed oxygen atoms in the 12-membered ring is 0.995 nm; the distance between opposed oxygen atoms situated in positions between two 12-membered rings is 1.12 nm. In the orthorhombic representation, which is obtained by copying the hexagonal cell using the translation vector $(0.5 \cdot a, a \sin 60°, 0)$, the cell constant in the y-direction is $b = 2.3774$ nm. Along the z-direction, a channel length of $L = 64$ sites was chosen. Within the cell length, c, two neopentane molecules can fit in a channel. Therefore, the unit cell was copied 32 times and an additional layer of oxygen atoms forming the 12-membered rings was added at one side to complete the L sites. The distance between the outer layers of oxygen atoms then is $L(c/2) = 27.15$ nm.

2.2. Spherical Model of Neopentane. The spherical model of neopentane is derived from a five-center model which uses the common united-atom approximation; that is, each CH_3 group, as well as the central carbon atom, is considered to be one Lennard-Jones center of interaction. The interaction parameters for the nonbonded interactions have been taken from refs 26−28. In ref 26, the σ and ϵ values are given for the single atoms or united atoms in neopentane. The Lorentz−Berthelot rules

$$\epsilon_{kl} = \sqrt{\epsilon_k \epsilon_l}, \quad \sigma_{kl} = \sigma_k + \sigma_l \tag{4}$$

are applied to obtain parameters for the interaction of unlike atoms.

The constants from ref 29 are used for the internal vibrations of neopentane. The potentials are in harmonic approximation

$$U_S = \frac{k_S}{2}(r - r_0)^2, \quad U_\Theta = \frac{k_\Theta}{2}(\Theta - \Theta_0)^2 \tag{5}$$

The constants are $k_\Theta = 590$ kJ/(mol·rad^2) for the bending angle with $\Theta_0 = 109.5° = 1.911$ rad and $k_S = 2613$ kJ/(mol·Å^2) for the bond stretching with $r_0 = 1.539$ Å.

To obtain a spherical approximation for the potential landscape experienced by any given particle (e.g., a lattice atom), close to the tetrahedral neopentane molecule, an integration over all directions could be carried out. In our opinion, this unbiased procedure may be improved by weighting different directions with respect to their frequency of occurrence in an average MD trajectory. Therefore, the spherical average has been calculated following the procedure used in ref 30 for methane. In each time step of an MD simulation run, the distance of the center of mass of each pair of neopentane molecules and the sum of all pair interaction energies of the mutual interaction of atoms

TABLE 1: Lennard-Jones Potential Parameters Used in the MD Simulation

interaction	σ/Å	ϵ/kJ mol^{-1}
C−C	3.800	0.2093
C−O	3.203	0.2300
CH_3−CH_3	3.960	0.6071
CH_3−O	3.600	0.6651
CH_3−C	3.880	0.3565
C_5H_{12}−C_5H_{12}	5.049	2.562
C_5H_{12}−O	4.234	1.126

of these two molecules are stored. At the end of the run, the average value of each sum of pair energies belonging to a given distance is taken. Analogously, the average potential between the five-center neopentane molecules and the oxygen atoms of the lattice was evaluated. From the resulting average potential curves, which have a shape similar to the Lennard-Jones potential, we chose the distance of the zero-crossing as the σ-parameter and the minimum value as the ϵ-parameter of the Lennard-Jones interaction. The values are given in Table 1.

2.3. An Analytical Potential Function for Neopentane in $AlPO_4$-5. With the approximation as a spherical particle, the potential energy of the neopentane molecule is reduced to a function of the three spatial coordinates (x, y, z). Making use of the periodicity of the crystal, it is possible to construct an analytical function, $E(x, y, z)$, that can be fitted to the potential energy landscape. The advantage of an analytical function for the potential energy is that it avoids the computation of hundreds of pair interactions between the particle and the lattice. Hence, the calculation of the force of the adsorbent is accelerated by a factor equal to the number of atoms of the adsorbent, which are usually taken into account. This number is, on average, usually in a range between 100 and 1000, depending, for example, on the cutoff radius of the interaction.

The analytical potential describes one single channel which is opened at both sides to a rectangular box describing the gas phase. The accessible space in the channel and the gas phase is described using repulsive forces of an r^{-12} distance dependency. The channel, which is aligned along the z-axis, is modeled as a tube with a sinusoidally varying diameter. At the channel openings, the diameter of the channel is extended to infinity. To limit the gas phase volume, additional repulsive walls are set in the x- and y-directions. These walls must be far enough from the channel entrance to guarantee a bulk gas phase in the entrance region, that is, to exclude static correlations in the density by interference of the influences of the gas box walls and the channel entrance on the density. On the other hand, with regard to the computational costs, the size of the gas phase needs to be limited. Both requirements are sufficiently fulfilled by the choice of a distance of 2 nm between the channel axis and the additional walls.

The attractive forces of the adsorbent are added to the repulsive forces of the channel walls. Inside the channel, the adsorption energy is modeled by a constant negative contribution of $U_{\min} < 0$ to the potential energy. This contribution is gradually reduced to zero in the transition region between the channel and the gas phase. Furthermore, the potential energy at an adsorption site is reduced and the energy barrier between adsorption sites is increased by adding a sinusoidal potential with an amplitude of $U_{\sin}$.

The characterizing potential parameters $U_{\min}$ and $U_{\sin}$ as well as the diameter of the tube have been adjusted to reproduce the potential that is obtained from the sum of pair interactions between the spherical neopentane and the oxygen atoms of the lattice. For the latter calculation, a cutoff radius of 1.45 nm

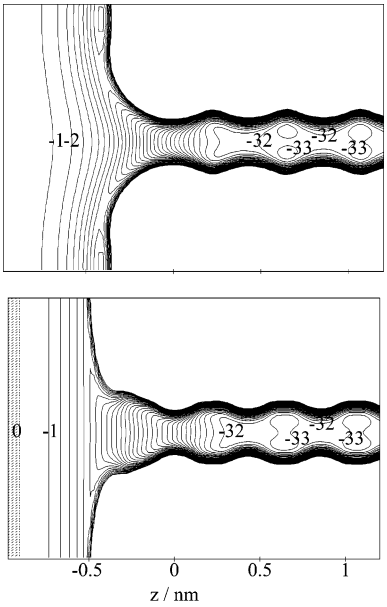

Figure 1. Comparison between the potential that is obtained from the sum of Lennard-Jones pair interactions between the spherical neopentane and the oxygen atoms of the lattice (top) and the fitted analytical potential energy function (bottom). The specified values of the potential are in kilojoules per mole.

was used together with shifted forces. It is essential to note that the heat of adsorption is more sensitive to the choice of the cutoff radius of the Lennard-Jones potential than the force field inside the zeolite channels. With respect to the large number of lattice oxygen atoms, this effect is important for the dynamics of particles leaving or entering the crystal. Therefore, the cutoff radius has to be chosen larger than in MD that covers only molecules inside zeolite crystals. With the cutoff radius used, we found a value of $|U_{\min}| = 32.7$ kJ/mol. A comparison between the atomistic and analytical potential energy landscapes is shown in Figure 1.

2.4. Variations of the Potential. In addition to the potential of neopentane in $AlPO_4$-5, where the potential barrier between adjacent minima in the channel ($\approx$3 kJ/mol) is small compared to the adsorption energy, we examined two further physical situations: (1) an increased internal barrier, which would describe a situation where the pathway between the adjacent adsorption sites leads through a more narrow region (e.g., a 10-membered ring), and (2) an increased internal barrier and, additionally, a reduced adsorption energy, so that the energy barriers in the channel are as high as the barrier to escape the channel. The variations of the potential could be achieved by simply multiplying $U_{\min}$ and $U_{\sin}$ by the factors $f_{U_{\min}}$ and $f_{U_{\sin}}$, respectively. In case 1, $f_{U_{\min}} = 1$ and $f_{U_{\sin}} = 20$ were used, and in case 2, $f_{U_{\min}} = 0.3$ and $f_{U_{\sin}} = 20$ were used. A comparison between the three potential functions is given in Figure 2. The figure shows the effective potential energy

$$E_{\text{pot,eff}}(z) = \frac{\int_x\int_y E_{\text{pot}}(x, y, z)\, \exp\{-\beta E_{\text{pot}}(x, y, z)\}\, \mathrm{d}x\, \mathrm{d}y}{\int_x\int_y \exp\{-\beta E_{\text{pot}}(x, y, z)\}\, \mathrm{d}x\, \mathrm{d}y} \quad (6)$$

along the channel axis. $E_{\text{pot,eff}}(z)$ is evaluated from the simulations.

2.5. Simulation Details. The system is considered at a desired site occupancy of $\theta = 0.5$ for comparison with previous Monte Carlo simulations[19] at the same occupancy. In preliminary simulations, we have tried to find a suitable simulation tem-

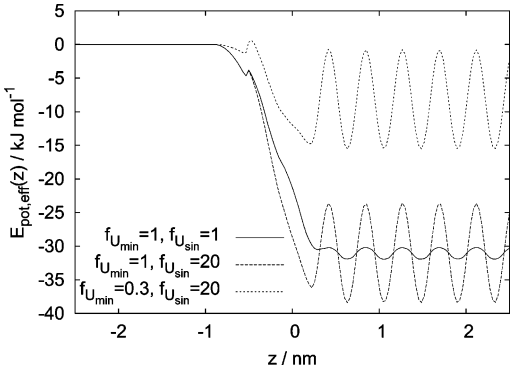

Figure 2. Effective potential, $E_{pot,eff}$, at the opening of the channel for the three considered potential functions. The potential with $f_{U_{min}} = 1$ and $f_{U_{sin}} = 1$ is given for neopentane in $AlPO_4$-5.

perature allowing fast intracrystalline diffusion and a possibility to keep the number of guest molecules needed for $\theta = 0.5$ sufficiently small. This was achieved for neopentane in $AlPO_4$-5 at a temperature of $T = 590$ K. The pressure, p, in the gas phase of the considered system was $\approx$2 MPa. This value is estimated from the particle density $n = 0.233$ nm^{-3} in the gas phase assuming an ideal gas where $p = nk_BT$ holds; k_B is the Boltzmann constant. At lower temperature, the diffusion becomes too slow to permit observation of tracer exchange up to the desired degree.

We have checked, for each potential function used, for the number of particles in the system needed to achieve sorption equilibrium at an occupation number close to $\theta = 0.5$. (Due to the integer number of particles in the system, the actual value of θ deviates, in general, from the desired value.) The durations of these simulations ensured a complete exchange of the initial particles. To start the production simulations as close as possible to an equilibrium value of $\theta = 0.5$, initially 32 particles were placed randomly inside the channel, whereas the remaining particles were placed randomly outside the channel in the gas phase. After equilibrating the system for 1 ns, production runs of 500 ns were carried out.

A time step of $h = 10$ fs was found to be appropriate due to the high mass of the particle. Since the energy exchange with the zeolite lattice is missing, a virtual heat bath is introduced by the method of Kast et al.[31,32] In this method, the particles experience (additionally to their mutual interaction) virtual central collisions with light virtual hard-sphere bath particles. For the present simulations, a bath particle mass of 0.02 g/mol was on one hand sufficiently large to ensure an equal temperature in the whole system and on the other hand small enough to leave even such sensitive quantities such as the velocity autocorrelation function of the neopentane molecules uninfluenced.

3. Evaluation

3.1. Coarse-Graining of the Molecular Movement. The movement of the particles may be coarse-grained into hops between adsorption sites, that is, regions where the residence probability is high compared to the pathway between these regions. The trajectories of the particles can therefore be stored in a digitalized format which has a number of advantages, as we will point out below. Within the unit cell of $ALPO_4$-5, two spacious regions are separated from each other by a more narrow region formed by the ring containing 12 oxygen atoms. Furthermore, the deepest minima of the potential energy are found in these spacious regions, and therefore, they are considered as adsorption sites in the following.

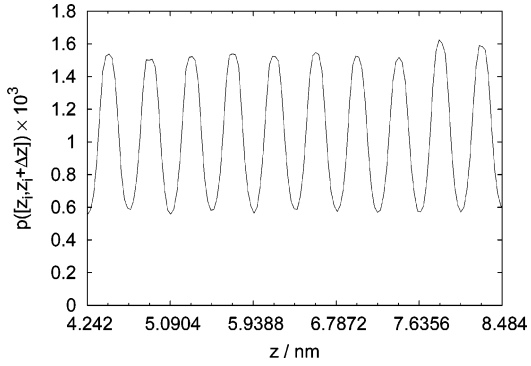

Figure 3. Adsorption sites in the channel: The plot shows the probability, p, of finding a particle in an interval $[z_i, z_i + \Delta z]$ on the z-axis in a central part of the channel; $\Delta z = 0.032$ nm. The calculation was performed for the potential of neopentane in $AlPO_4$-5 at a temperature of $T = 590$ K.

Figure 3 shows the probability to find a particle as a function of the position on the z-axis. Minima and maxima are found periodically in the channels. The minima are situated at the positions of the 12-membered rings with a distance of $\lambda = c/2 = 0.4242$ nm between neighboring minima. The calculation was performed for the potential of neopentane in $AlPO_4$-5 at a temperature of $T = 590$ K. The adsorption sites are sufficiently well defined also in this potential where the barriers between the adsorption sites have a height of only a few kilojoules per mole. For the other two potentials used, the adsorption sites are, of course, even more pronounced due to the higher energy barrier between them. Therefore, we have not shown them in the plot.

For the calculation of the tracer-exchange profiles, only the information about hops between these adsorption sites is necessary. After each time step of the simulation, the z-coordinate of the molecules was assigned to the number of the respective adsorption site, to one of the outer surfaces, or to the gas phase. The particle trajectories were stored for further evaluation using the coarse-grained format. Beginning with the initial site positions of each particle, in the following, only changes between the sites were registered together with the current MD step number. Compared to the method of recording particle coordinates of fixed time intervals, the coarse-grained trajectories have the advantage that the information on every jump between the sites is registered and can be used for further data processing without the need for oversized data files.

3.2. Tracer-Exchange Profiles. In the tracer-exchange experiment, identical particles which carry different labels are considered. In the initial situation, all particles in the channel are assumed to be labeled and all particles outside are assumed to be unlabeled. As soon as a particle leaves the channel, it is assumed that it is carried away by a stream; therefore, only the unlabeled particles can enter the channel. In the MD simulation, we have a constant total number of particles. For this reason, we may remove the label from every particle leaving the channel. After sufficiently large time, all particles will be unlabeled.

The point when a particle is considered to be desorbed (and will therefore lose the label) can be defined in two different ways. According to the first definition, the particle loses the label when it leaves the channel and reaches the outer surface of the adsorbent so that another particle may occupy the vacancy in the channel. According to the second definition, a molecule is considered as desorbed if it leaves the channel and, *furthermore*, if it manages to leave the surface and to move to the gas phase. In the second case, a particle may reenter the

channel without moving to the gas phase and keep the label. We have compared the tracer-exchange profiles for both definitions and found only a slightly lower degree of exchange for the second definition compared to the first definition for the temperature of the simulations ($T = 590$ K). The definition that a particle is considered as desorbed if it leaves the channel has also been used in refs 14, 18, and 19 which we seek to compare our results to. For this reason, we decided to use this definition also in the present work.

The tracer-exchange concentration profiles, $C(x, t)/C_0$, where C_0 is the concentration required to maintain equilibrium with the surrounding atmosphere, are calculated from the coarse-grained trajectory by building for each site i at position x the ratio of the number $N_{ex}(i)$ of the exchanged, unlabeled particles and the total number $N_{tot}(i)$ of particles at site i. In other words, $N_{ex}(i)/N_{tot}(i)$ is the probability that a particle found at site i is an exchanged one. We averaged $N_{ex}(i)$ and $N_{tot}(i)$ over 500 independent simulations, each considering a single channel, and, furthermore, over the simulation time. The channel average is essential, because, especially in the case of single-file diffusion, long-term correlations occur within one channel.

The tracer-exchange profiles are compared to the analytical solution of the diffusion equation for the situtation of surface evaporation.[33] Assuming that the flux, J, through the crystal surface is proportional to the difference between the concentration required to maintain equilibrium with the surrounding atmosphere, C_0, and the actual concentration within the channel, C_s, one obtains for Fick's second law the boundary condition

$$J = \alpha(C_0 - C_s) \tag{7}$$

where α is the proportionality constant. If the channel $-l < x < l$ (where $2l = L(c/2)$ is the total length of the channel and $c = 8.484 \times 10^{-10}$ m is the cell constant of $AlPO_4$-5 in the z-direction which is the width of two sites) is initially at a uniform concentration, C_2, and the law of exchange of the type of eq 7 holds on both sides, the solution is[33]

$$\frac{C(x, t) - C_2}{C_0 - C_2} = 1 - \sum_{n=1}^{\infty} \frac{2\Lambda \cos(\beta_n x/l) \exp\{-\beta_n^2 Dt/l^2\}}{(\beta_n^2 + \Lambda^2 + \Lambda)\cos\beta_n} \tag{8}$$

where the β_n's are the positive roots of $\beta \tan \beta = \Lambda$; $\Lambda = l\alpha/D$ is a dimensionless parameter. Under the conditions considered in this paper, $C_2 = 0$.

In our previous paper, ref 19, the profiles were compared to the solutions for the case of infinite permeability; that is, the boundary conditions $C(-l) = C(l) = C_0$ hold for $t > 0$. The solution for this case is

$$\frac{C(x, t)}{C_0} = 1 - \frac{4}{\pi} \sum_{n=0}^{\infty} \frac{(-1)^n}{2n+1} \cos\left\{\frac{(2n+1)\pi x}{2l}\right\} \exp\left\{-\frac{(2n+1)^2 \pi^2 Dt}{4l^2}\right\} \tag{9}$$

and is *equivalent* to eq 8 for the special case $\alpha \rightarrow \infty$. Fitting the profiles to both solutions, we found practical numeric coincidence between both solutions for high values of α and a fixed value for D, as will be described in more detail in the next section.

4. Results

For sufficiently large times, the diffusion process in finite single-file systems far from the system boundaries is expected to obey the laws of normal diffusion with the diffusivity D_s (eqs 2 and 3). As a result, the tracer-exchange concentration profiles far from the boundaries are expected to be in agreement with the corresponding profiles observed for normal diffusion. This expectation has been confirmed by recent dynamic MC simulations,[19] which have also revealed a significant boundary effect, that is, deviations of the profiles near boundaries of single-file systems from the corresponding profiles for normal diffusion. This boundary effect is the main focus of the present work. In the following, we present the results of MD simulations showing the tracer-exchange concentration profiles for the cases of normal and single-file diffusion. The conditions of normal diffusion were met by making the σ-parameter smaller than in the case of single-file diffusion and maintaining all other system parameters unchanged. This allows the particles to exchange their positions in the channel so that the conditions of normal diffusion are achieved. Furthermore, the profiles are fitted to eq 8 which holds for the case of normal diffusion under the considered conditions as described above.

Figure 4 shows the tracer-exchange profiles obtained from the simulations. Different columns show the results for the three different potentials used, that is, for the reference system neopentane in $AlPO_4$-5 (left) and for the cases when the potentials are varied by using the factors $f_{U_{min}}$ and $f_{U_{sin}}$ (middle and right). For each potential, three different durations, t, of the tracer-exchange experiment, with the respective degrees of exchange, $\gamma(t)$, are given in different graphs. In each graph, the profiles from the simulations obtained for normal and single-file diffusion are given for approximately the same degree of exchange. Obviously, much larger exchange times are needed for single-file than for normal diffusion in order to meet this condition.

In all cases, the pairs of profiles for normal and single-file diffusion clearly differ from each other. The profiles for single-file diffusion show higher concentration values at the boundaries and lower values in the center of the channel compared to normal diffusion. However, the inner part of the profiles for single-file diffusion behaves like the profiles for normal diffusion and can be fitted by eq 8 if a smaller channel length is assumed. Hence, the number of sites, L, was used as an additional fitting parameter. The clearest results with respect to the deviations of the profiles near the boundaries are obtained for the potential employing a higher internal barrier and a lower adsorption energy (right column in Figure 4). Under this condition, the same type of boundary effect as that observed previously by using dynamic MC simulations[19] can be clearly seen: the concentration of the unlabeled particles near the channel boundaries is always closer to the equilibrium one in the case of single-file diffusion than in the case of normal diffusion. This implies that under the conditions of single-file diffusion the molecular exchange between the channel regions near boundaries and the gas phase occurs faster than that predicted by the laws of normal diffusion with the diffusivity far from the channel margins. The concentration profiles in the middle and left columns of Figure 4 show the same tendency. In the latter profiles, a relatively high evaporation barrier leads to an additional decrease of the concentration of the labeled particles near the boundaries for both single-file and normal diffusion (Figure 4).

All profiles are fitted by eq 8, and the values of the diffusion coefficient, D, the permeability, α, and, in the case of single-file diffusion, the number of sites in the channel, L, are listed

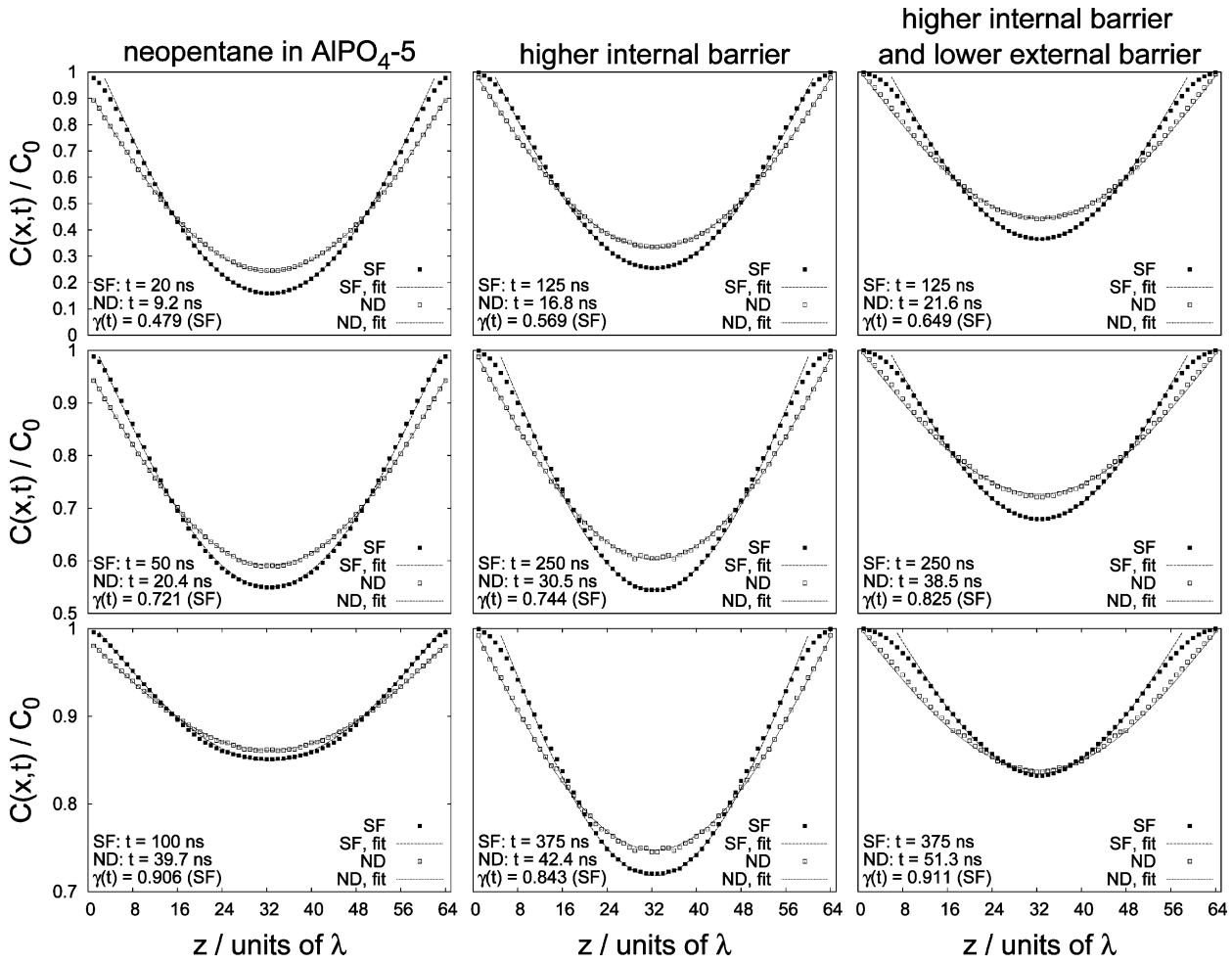

Figure 4. Tracer-exchange concentration profiles of unlabeled (exchanged) particles for single-file diffusion (SF) in comparison to normal diffusion (ND) for approximately the same degree of exchange, γ. The value of γ is specified for the case of single-file diffusion. The *x*-scale is given in units of the distance between two neighboring sites, $\lambda = c/2 = 0.4242$ nm. The best fits by eq 8 are added; the respective parameters are given in Table 2. Note that the channel length, *L*, was considered as a variable when fitting the profiles obtained for single-file diffusion. Each column shows the results for the indicated potentials, and in each row, another degree of exchange, γ, is given (note that the *y*-range varies between the three rows).

TABLE 2: Parameters of eq 8 Obtained from the Fit of the Tracer-Exchange Profiles Shown in Figure 4 (SF, Single File; ND, Normal Diffusion)

type	$f_{U_{min}}$	$f_{U_{sin}}$	t/ns	$\gamma(t)$	$D/10^{-10}$ m^2 s^{-1}	α/m s^{-1}	L/sites
SF	1	1	20	0.479	13.1	(100)	60
			50	0.721	14.5	(100)	62
			100	0.906	15.0	(100)	62
SF	1	20	125	0.569	2.60	(100)	58
			250	0.744	2.35	(100)	56
			375	0.843	2.30	(100)	56
SF	0.3	20	125	0.649	2.95	(100)	54
			250	0.825	2.93	(100)	54
			375	0.911	2.68	(100)	52
ND	1	1	9.2	0.481	48.0	4.6	64
			20.4	0.721	48.0	4.6	64
			39.7	0.905	48.3	4.6	64
ND	1	20	16.8	0.570	29.1	24.4	64
			30.5	0.745	29.0	24.4	64
			42.4	0.838	29.0	24.4	64
ND	0.3	20	21.6	0.649	28.8	(100)	64
			38.5	0.828	30.0	(100)	64
			51.3	0.899	30.2	(100)	64

in Table 2. The values for α given in brackets are only estimates. For these values, the solutions of eqs 8 and 9 are practically identical.

From the fitting, diffusion coefficients in the range of $(1.4 \pm 0.1) \times 10^{-9}$ m^2 s^{-1} are obtained for neopentane in $AlPO_4$-5 under the considered system conditions. A reasonable fit by eq 8 is possible if lower values of the channel length, *L*, are chosen. The fits of the profiles for normal diffusion yield higher diffusion coefficients, $D = (4.8 \pm 0.1) \times 10^{-9}$ m^2 s^{-1}, and a value of $\alpha = 4.6$ ms^{-1}. In this case, eq 8 perfectly describes the profiles; thus, *L* is unchanged. Comparison of the diffusivities reported above indicates that, by imposing the conditions of single-file diffusion, which prohibits an exchange of the relative positions of particles in single-file channels, a surprisingly small decrease in the value of the diffusion coefficient results. This observation needs further study.

We attribute the observed boundary effects for single-file diffusion to an interplay of the two different diffusion mechanisms occurring in parallel, that is, the center-of-mass diffusion of the whole chain of labeled particles in the channel, which obeys the laws of normal diffusion, and the diffusion of the individual labeled particles with respect to the center of mass of the labeled particles in any particular channel. The latter type of movement is the anomalous diffusion, which for suffuciently short times can be expected to conform with single-file diffusion.[15] For short times, the mean square displacement of the particles due to single-file diffusion is higher than the contribution of the center-of-mass diffusion, thus leading to a significant increase of the rate of molecular exchange near the

boundaries in comparison to the case of the "rigid" chain of particles described by the latter mechanism.

5. Conclusions

Using molecular dynamics simulations of diffusion of guest molecules in channels of model zeolite systems, we have observed that, under the conditions of single-file diffusion, the tracer-exchange profiles show a boundary effect; that is, at the boundaries, the equilibrium molecular concentration is reached faster than in the case of normal diffusion when comparing concentration profiles with the same degree of exchange. The observed boundary effect is attributed to the interplay of the following two types of movements in single-file systems: (i) center-of-mass diffusion describing the movement of the labeled particles in each channel as that of the rigid chain, which implies the same displacements for all particles in the chain as well as for the center of mass of the chain, and (ii) anomalous (i.e., single file for short times) diffusion of individual particles in the channels with respect to the center of mass of the chain. Mechanism ii leads to an acceleration of molecular exchange near channel boundaries in comparison to that expected for the normal diffusion according to mechanism i.

Acknowledgment. The authors thank the Deutsche Forschungsgemeinschaft for financial support given in the frame of the SPP 1155. Numerous discussions with Prof. J. Kärger are gratefully acknowledged.

Supporting Information Available: Table of the lattice atom positions. This material is available free of charge via the Internet at http://pubs.acs.org.

References and Notes

(1) Baerlocher, C.; Meier, W. M.; Olson, D. H. *Atlas of Zeolite Framework Types*, 5th ed.; Elsevier: Amsterdam, The Netherlands, 2001.
(2) Ebbesen, T. W., Ed. *Carbon Nanotubes: Preparation and Properties*; CRC Press: Boca Raton, FL, 1997.
(3) Roux, B. In *Computer Modelling in Molecular Biology*; Goodfellow, J. M., Ed.; VCH: New York, 1995.
(4) Hahn, K.; Kärger, J.; Kukla, V. *Phys. Rev. Lett.* **1996**, *76*, 2762−2765.
(5) Kukla, V.; Kornatowski, J.; Demuth, D.; Girnus, I.; Pfeifer, H.; Rees, L. V. C.; Schunk, S.; Unger, K. K.; Kärger, J. *Science* **1996**, *272*, 702−704.
(6) Jobic, H.; Hahn, K.; Kärger, J.; Bée, M.; Noack, M.; Girnus, I.; Tuel, A.; Kearley, G. J. *J. Phys. Chem. B* **1997**, *101*, 5834−5841.
(7) Wei, Q. H.; Bechinger, C.; Leiderer, P. *Science* **2000**, *287*, 625−627.
(8) Lutz, C.; Kollmann, M.; Bechinger, C. *Phys. Rev. Lett.* **2004**, *93*, 026001−1−4.
(9) Fedders, P. A. *Phys. Rev. B* **1978**, *17*, 40−46.
(10) Kärger, J. *Phys. Rev. A* **1992**, *45*, 4173−4174.
(11) Kollmann, M. *Phys. Rev. Lett.* **2003**, *90*, 180602−1−4.
(12) Keffer, D.; McCormick, A. V.; Davis, H. T. *Mol. Phys.* **1996**, *87*, 367−387.
(13) Hahn, K.; Kärger, J. *J. Phys. Chem. B* **1998**, *102*, 5766−5771.
(14) Nelson, P. H.; Auerbach, S. M. *J. Chem. Phys.* **1999**, *110*, 9235−9243.
(15) Demontis, P.; Stara, G.; Suffritti, G. B. *J. Chem. Phys.* **2004**, *120*, 9233−9244.
(16) Mon, K. K.; Percus, J. K. *J. Chem. Phys.* **2002**, *117*, 2289−2292.
(17) Pal, S.; Srinivas, G.; Bhattacharyya, S.; Bagchi, B. *J. Chem. Phys.* **2002**, *116*, 5941−5950.
(18) Nelson, P. H.; Auerbach, S. M. *Chem. Eng. J.* **1999**, *74*, 43−56.
(19) Vasenkov, S.; Kärger, J. *Phys. Rev. E* **2002**, *66*, 0526011−0526014.
(20) Corma, A. *J. Catal* **2003**, *216*, 298−312.
(21) Tao, Y.; Kanoh, H. *J. Am. Chem. Soc.* **2003**, *125*, 6044−6045.
(22) Lehmann, E.; Chmelik, C.; Scheidt, H.; Vasenkov, S.; Staudte, B.; Kärger, J.; Kremer, F.; Zadrozna, G.; Kornatowski, J. *J. Am. Chem. Soc.* **2002**, *124*, 8690−8692.
(23) Lehmann, E.; Vasenkov, S.; Kärger, J.; Zadrozna, G.; Kornatowskic, J. *J. Chem. Phys.* **2003**, *118*, 6129−6132.
(24) Ikeda, T.; Miyazawab, K.; Izumic, F.; Huangd, Q.; Santorod, A. *J. Phys. Chem. Solids* **1999**, *60*, 1531−1535.
(25) Kirstein, J. Diffusionsmessungen auf Einzelmolekülbasis in nanoporösen M41S Molekularsieben und Modellierung der $AlPO_4$-5 Struktur. Master's Thesis, Ludwig-Maximilians-Universität München, 2002.
(26) Jorgensen, W. L.; Madura, J. D.; Swenson, C. J. *J. Am. Chem. Soc.* **1984**, *106*, 6638−6646.
(27) Burkert, U.; Allinger, N. L. *Molecular Mechanics*; American Chemical Society: Washington, DC, 1982.
(28) Furukawa, S.; McCabea, C.; Nitta, T.; Cummings, P. *Fluid Phase Equilib.* **2002**, *194*, 309−317.
(29) Weaver, J. F.; Madix, R. J. *J. Chem. Phys.* **1999**, *110*, 10585−10598.
(30) Fritzsche, S.; Wolfsberg, M.; Haberlandt, R. *Chem. Phys.* **2003**, *289*, 321−333.
(31) Kast, S.; Nicklas, K.; Bär, H.-J.; Brickmann, J. *J. Chem. Phys.* **1993**, *100*, 566−576.
(32) Kast, S.; Brickmann, J. *J. Chem. Phys.* **1996**, *104*, 3732−3741.
(33) Crank, J. *The Mathematics of Diffusion;* Clarendon Press: Oxford, U.K., 1956.